

Nonmuscle myosin 2 regulates cortical stability during sprouting angiogenesis

Xuefei Ma^{a,*}, Yutaka Uchida^{b,†}, Tingyi Wei^a, Chengyu Liu^c, Ralf H. Adams^d, Yoshiaki Kubota^e, J. Silvio Gutkind^f, Yoh-suke Mukoyama^b, and Robert S. Adelstein^{a,*}

^aLaboratory of Molecular Cardiology; ^bLaboratory of Stem Cell and Neurovascular Biology, and ^cTransgenic Core Facility, National Heart, Lung, and Blood Institute, National Institutes of Health, Bethesda, MD 20892-1762;

^dDepartment of Tissue Morphogenesis, Max Planck Institute for Molecular Biomedicine and Faculty of Medicine, University of Munster, D-48149 Munster, Germany; ^eDepartment of Anatomy, Keio University School of Medicine, 35 Shinanomachi, Shinjuku-ku, Tokyo 160-8582, Japan; ^fMoore's Cancer Center, University of California, San Diego, La Jolla, CA 92093

ABSTRACT Among the three nonmuscle myosin 2 (NM2) paralogs, NM 2A and 2B, but not 2C, are detected in endothelial cells. To study the role of NM2 in vascular formation, we ablate NM2 in endothelial cells in mice. Ablating NM2A, but not NM2B, results in reduced blood vessel coverage and increased vascular branching in the developing mouse skin and coronary vasculature. NM2B becomes essential for vascular formation when NM2A expression is limited. Mice ablated for NM2B and one allele of NM2A develop vascular abnormalities similar to those in NM2A ablated mice. Using the embryoid body angiogenic sprouting assay in collagen gels reveals that NM2A is required for persistent angiogenic sprouting by stabilizing the endothelial cell cortex, and thereby preventing excessive branching and ensuring persistent migration of the endothelial sprouts. Mechanistically, NM2 promotes focal adhesion formation and cortical protrusion retraction during angiogenic sprouting. Further studies demonstrate the critical role of Rho kinase-activated NM2 signaling in the regulation of angiogenic sprouting *in vitro* and *in vivo*.

Monitoring Editor

Alpha Yap
University of Queensland

Received: Mar 6, 2020

Revised: Jun 9, 2020

Accepted: Jun 12, 2020

INTRODUCTION

Collective cell migration requires highly orchestrated, mechanically coupled migratory behavior which coordinates regulation of cell–cell adhesion, intercellular communication, and cell contractility to ensure efficient directional cell migration (Mayor and Etienne-Manneville, 2016; Park *et al.*, 2016). The leader cells positioned at the front of the sprout generate lamellipodial and filopodial protrusions that sense, lead, and power the migration. The follower cells proceed by cell–cell contact. In addition, cell–cell contact inhibition

of locomotion prevents the follower cells from scattering. Angiogenesis, the process of neovascular formation from preexisting blood vessels through collective endothelial cell sprouting in response to various angiogenic stimuli, is essential for many physiological and pathological conditions, including animal development, wound healing, and tumor formation (Phng and Gerhardt, 2009; Eilken and Adams, 2010; Carmeliet and Jain, 2011). Collective endothelial cell migration is a critical event for angiogenesis. In response to angiogenic stimuli, endothelial cells polarize, initiate sprouts, and migrate toward the angiogenic stimulus (such as vascular endothelial growth factor [VEGF] and fibroblast growth factor [FGF]). All these aspects rely on the integrated dynamic regulation of cell adhesion and the cytoskeleton. VEGF induces polarized cell elongation by decreasing VE-cadherin concentration at junctions, triggering polarized formation of actin-driven, junction-associated intermittent lamellipodia (JAIL) and thereafter endothelial cell sprouting (Cao *et al.*, 2017). *In vivo* studies from both mice and zebrafish show that loss of VE-cadherin at endothelial cell–cell junctions results in excessive angiogenic sprouting associated with disrupted actin filaments at these junctions (Abraham *et al.*, 2009; Gaengel *et al.*, 2012; Sauter *et al.*, 2014). Dynamic endothelial

This article was published online ahead of print in MBoc in Press (<http://www.molbiolcell.org/cgi/doi/10.1091/mbc.E20-03-0175>) on June 17, 2020.

[†]Present address: Department of Immunology and Cell Biology, Graduate School of Medicine and Frontier Biosciences, Osaka University, Osaka 565-0871, Japan.

*Address correspondence to: Xuefei Ma (max@nhlbi.nih.gov); Robert S. Adelstein (adelster@nhlbi.nih.gov).

Abbreviations used: E, embryonic day; EB, embryoid body; NM, nonmuscle myosin; pPaxillin, phospho-paxillin.

© 2020 Ma *et al.* This article is distributed by The American Society for Cell Biology under license from the author(s). Two months after publication it is available to the public under an Attribution–Noncommercial–Share Alike 3.0 Unported Creative Commons License (<http://creativecommons.org/licenses/by-nc-sa/3.0>).

“ASCB®,” “The American Society for Cell Biology®,” and “Molecular Biology of the Cell®” are registered trademarks of The American Society for Cell Biology.

cell–cell adhesions during angiogenic sprouting are associated with the activity of nonmuscle myosin 2 (NM2), a member of the conventional myosin 2 family, which is ubiquitously expressed both in muscle and nonmuscle cells in vertebrates. Inhibition of myosin ATPase activity by the NM2 inhibitor blebbistatin or the Rho kinase inhibitor Y27632 disrupts VE–cadherin mediated endothelial cell–cell adhesion associated with increased sprouting activity (Abraham *et al.*, 2009; Wimmer *et al.*, 2012; Cao *et al.*, 2017). NM2 activity is also involved in endothelial cell rearrangement during sprout elongation (Angulo-Urarte *et al.*, 2018). Recently, it was shown that application of blebbistatin or Y27632 and deletion of the NM2A paralog in endothelial cells disrupts cell–cell adhesion and results in endothelial cell scattering in a 3D angiogenic sprouting culture of human umbilical vein endothelial cells (Yoon *et al.*, 2019). In addition, the acute injection of blebbistatin into the developing postnatal mouse retina leads to increased numbers of detached endothelial cells at the migrating front of the developing retina vasculature (Yoon *et al.*, 2019). The role of NM2 in angiogenesis, however, has not been tested directly *in vivo* during animal development.

NM2 is composed of a pair of coiled-coil heavy chains with globular heads, and two pairs of myosin light chains (Heissler and Manstein, 2013; Ma and Adelstein, 2014). NM2 constitutes one of the most abundant cytoplasmic motor proteins, supporting various cellular functions in eukaryotic cells, such as cell division, cell migration, and cell adhesion. Three paralogs of NM2, namely NM2A, 2B, and 2C, have been identified based on differences in their heavy chains, which are the products of three different genes (*Myh9*, *Myh10*, and *Myh14*, respectively) located on different chromosomes in humans and mice (Berg *et al.*, 2001; Golomb *et al.*, 2004). The expression level of each NM2 varies in different organs and cells and is also regulated during development in mice. The three NM2s exert overlapping as well as unique functions in mouse development. Mice ablated for NM2A die very early in development by embryonic day (E)6.5 before gastrulation, due to a failure in visceral endoderm formation (Conti *et al.*, 2004). Mice ablated for NM2B die by E14.5 from severe defects in brain and heart development (Tullio *et al.*, 1997, 2001). NM2C-ablated mice have no obvious detectable abnormalities (Ma *et al.*, 2010). Both NM2B and 2C can replace NM2A *in vivo*, supporting cell–cell adhesion and functional visceral endoderm formation, but cannot replace NM2A during placental vascular formation in mouse embryonic development (Wang *et al.*, 2010; Zhang *et al.*, 2018). In addition, NM2 paralogs may function together by forming heteromyosin filaments (Beach *et al.*, 2014; Shutova *et al.*, 2014). In most cases, mammalian cells express at least two NM2 paralogs. In developing mouse endothelial cells, NM2A and 2B, but not NM2C, are detected. Whether and how NM2 paralogs function together in the regulation of developmental processes such as blood vessel formation is not clear.

This study was designed to investigate the role of NM2A and 2B in vascular network formation during mouse development. The data presented in this report demonstrate that both NM2A and 2B are involved during embryonic blood vessel formation. This is accomplished using serial, endothelial cell–specific, and temporal ablations of various combination of NM2A and 2B during embryonic mouse development. These data also make use of an *in vitro* embryoid body angiogenic sprouting assay from NM2A and NM2B ablated mouse embryonic stem cells grown in 3D culture. Mechanistically, NM2A is essential for sprouting angiogenesis by maintaining the integrity of the cortical membrane through retraction of membrane protrusions, thereby ensuring persistent collective endothelial cell sprouting.

RESULTS

Ablation of nonmuscle myosin 2A, but not 2B, impairs vascular network formation in mice

To illustrate the expression of NM2A and 2B in the developing mouse vasculature, the back skins from mouse embryos that expressed EGFP-fused NM2A or 2B were dissected at embryonic day (E)14.5 and then wholemount stained with antibodies against GFP together with CD31 (a marker for endothelial cells). Supplemental Figure S1A displays the distribution of NM2A and 2B in the developing E14.5 mouse back skin. NM2A is predominantly detected in vascular endothelial cells (Supplemental Figure S1Aa) that costain with CD31 (Supplemental Figure S1Ab). NM2B is also detected in vascular endothelial cells, but is not as enriched as in endothelial cells (Supplemental Figure S1Ae) compared with other cells such as hair follicle cells (Supplemental Figure S1Ad, arrows). Panels S1Ac and S1Af show merged images of two channels. Staining using GFP antibodies also allows us to estimate the relative expression levels of NM2A and 2B in vascular endothelial cells *in vivo*. Supplemental Figure S1A shows that vascular endothelial cells expresses significantly more NM2A (Supplemental Figure S1a) than NM2B (Supplemental Figure S1d). Because NM2C is not detected in endothelial cells, our studies focus on the role of NM2A and 2B in vascular network formation.

We first individually ablated NM2A and 2B from endothelial cells in mice by crossing NM2A or NM2B floxed mice with Tie2-cre mice where the cre recombinase is expressed in all endothelial cells. E14.5 embryos ablated for NM2A (A^{Tie2}/A^{Tie2}) develop edema (Supplemental Figure S1Bb, red arrows) and hemorrhage (Supplemental Figure S1Bb, white arrows), indicating a leakage of the blood vessels in A^{Tie2}/A^{Tie2} mice, which is not observed in control A^{fllox}/A^{fllox} embryos (Supplemental Figure S1Ba). To evaluate the vascular phenotype of endothelial NM2A or 2B ablated mice, the vasculature in E14.5 mouse back skins was visualized by wholemount staining using antibodies to CD31. As shown in Figure 1, the vascular network in A^{Tie2}/A^{Tie2} mice is less mature, showing only a “chicken wire” capillary plexus (Figure 1b), and covers a reduced area of the back skin as compared with A^{fllox}/A^{fllox} littermates, which show a hierarchical vascular network (Figure 1a, arrows). To quantitate the extent of the blood vessel coverage, we measured the angle between the lines bordering the front edges of vascular sprouts in an open-book configuration of the back skin (a, b, dashed lines). The larger the angle, the lower the coverage. The average angle for control mice is $23 \pm 6^\circ$ ($n = 4$ mice). The average angle for A^{Tie2}/A^{Tie2} mice is $40 \pm 4^\circ$ ($n = 4$ mice), which is significantly larger than for the control mice ($p < 0.01$). In addition, A^{Tie2}/A^{Tie2} mice show abnormal clusters of endothelial cells at the middle of the back skin that are disconnected from centrally growing vascular sprouts (Figure 1d, yellow arrows). These clusters are not normally seen in control mice. Closer examination of the front of the vascular sprouts shows that wild-type sprouts are smooth, without obvious branches (Figure 1c, white arrows); A^{Tie2}/A^{Tie2} sprouts, however, contain multiple branches (Figure 1d, white arrows). Thus loss of NM2A results in vascular overbranching. Quantitation of branch points of the vascular networks from A^{fllox}/A^{fllox} and A^{Tie2}/A^{Tie2} mice using the AngioTool reveals a moderate, but significant increase in branch points in A^{Tie2}/A^{Tie2} mice (27 ± 1.5 per mm length) compared with the A^{fllox}/A^{fllox} mice (24.5 ± 2.7 per mm length; Supplemental Figure S2, $n = 4$ mice each, $p < 0.05$). Note that the developing back skin vascular sprouts remain in a centrally migrating pattern in the open-book configuration in both A^{Tie2}/A^{Tie2} and A^{fllox}/A^{fllox} embryos. This indicates that ablation of NM2A does not affect the directionality of the migrating vascular sprouts.

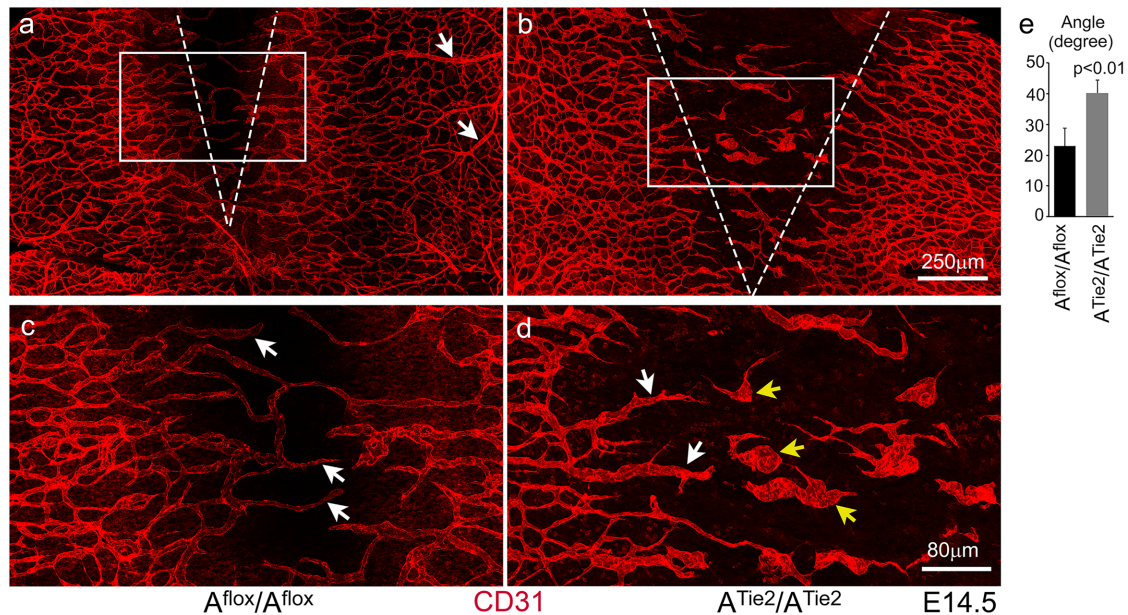


FIGURE 1: Abnormal blood vessel formation in A^{Tie2}/A^{Tie2} mouse back skins at E14.5. Wholemount confocal images of back skins dissected from A^{Tie2}/A^{Tie2} (b, enlarged in d) and A^{flox}/A^{flox} control (a, enlarged in c) mice at E14.5 stained with CD31 antibodies to reveal the developing vasculature (red) show that A^{Tie2}/A^{Tie2} mice have reduced blood vessel coverage, b, compared with A^{flox}/A^{flox} mice, a. A^{flox}/A^{flox} mice develop mature blood vessels—a, arrows, which are not seen in A^{Tie2}/A^{Tie2} mice, b. The dashed white lines in a and b depict a V-shaped area that has not been fully covered by blood vessels. A^{flox}/A^{flox} back skins develop smooth straight vascular sprouts toward the middle of the back—c, arrows. A^{Tie2}/A^{Tie2} back skins show vascular sprouts that contain multiple branches—d, white arrows. Isolated clusters of endothelial cells are observed in the middle of A^{Tie2}/A^{Tie2} back skins—d, yellow arrows—which are not seen in A^{flox}/A^{flox} mice, c. Panel e shows the quantification of average angles from A^{flox}/A^{flox} and A^{Tie2}/A^{Tie2} mouse back skins, $n = 4$ for each genotype.

In contrast, ablation of NM2B alone in endothelial cells shows no edema, no hemorrhage, and no obvious defects in blood vessel formation in the back skin at E14.5 (Figure 2b) compared with the control littermate (Figure 2a). As previously shown (Tullio *et al.*, 1997; Takeda *et al.*, 2003), although B^{-}/B^{-} mice (germline ablation of NM2B) develop severe defects in the heart and die by E14.5 during embryonic development with heart failure, no significant defects in blood vessel formation are found in these mice at E14.5 (Figure 2, e and f) compared with their control littermates (Figure 2, d and f). These data suggest that defective heart development does not affect the vascular network in the B^{-}/B^{-} back skin. Taken together these results show that NM2A, but not NM2B, is essential for vascular network formation in the developing mouse skin. Additionally, NM2A functions to prevent angiogenic sprouts from excessive branching during vascular network formation.

An auxiliary role for NM 2B in blood vessel formation during mouse development

As shown above, the development of blood vessels is compromised but not drastically disrupted in A^{Tie2}/A^{Tie2} mice. We thus hypothesize that NM2B is also functioning during vascular network formation, especially in A^{Tie2}/A^{Tie2} mice. To test this idea, we generated NM2A and 2B compound endothelial cell-ablated mice. Crossing a Tie2-Cre male with an $A^{flox}/A^{flox}; B^{flox}/B^{flox}$ female generated healthy heterozygous $A^{+}/A^{Tie2}; B^{+}/B^{Tie2}$ mice. Figure 2 shows the back skin vasculatures from littermates obtained by crossing an $A^{+}/A^{Tie2}; B^{+}/B^{Tie2}$ male with an $A^{+}/A^{+}; B^{flox}/B^{flox}$ female. $A^{+}/A^{Tie2}; B^{+}/B^{Tie2}$ mice, which express one copy of NM2A but no 2B, show abnormalities in vascular network formation. The back skin vasculature in these mice at E14.5 (Figure 2c) appears less mature and shows reduced coverage

compared with control littermates (Figure 2a). The average branch points for $A^{+}/A^{Tie2}; B^{+}/B^{Tie2}$ vasculatures is 27 ± 3 per mm length (Figure 2f, $n = 4$, $p < 0.05$), which is moderately increased compared with control $A^{+}/A^{+}; B^{flox}/B^{flox}$ vasculatures (Figure 2f, 23 ± 1 , $n = 4$). Note that defects in $A^{+}/A^{Tie2}; B^{+}/B^{Tie2}$ vasculatures are not as severe as those seen in A^{Tie2}/A^{Tie2} vasculatures. These results indicate that expression of one copy of NM2A is not sufficient to support normal blood vessel formation when NM2B is not expressed, while expression of one copy of NM2A plus one copy of NM2B is sufficient. Crossing $A^{+}/A^{Tie2}; B^{+}/B^{Tie2}$ males with $A^{flox}/A^{flox}; B^{flox}/B^{flox}$ females generated no live $A^{Tie2}/A^{Tie2}; B^{+}/B^{Tie2}$ and $A^{Tie2}/A^{Tie2}; B^{Tie2}/B^{Tie2}$ embryos at E12.5. At E10.5 the $A^{Tie2}/A^{Tie2}; B^{+}/B^{Tie2}$ embryo is smaller than the controls (Supplemental Figure S3c), and the $A^{Tie2}/A^{Tie2}; B^{Tie2}/B^{Tie2}$ embryo is significantly delayed in development with pericardial effusion (Supplemental Figure S3d, arrow). These results further support the importance of NM2B in endothelial cells during mouse development. Early embryonic death of $A^{flox}/A^{flox}; B^{Tie2}/B^{Tie2}$ double homozygous mice prevents further analyses of the vascular phenotypes in the skin.

Defects in blood vessel formation are not limited to the back skin. Mice ablated for NM2 in endothelial cells also show abnormalities in coronary vessel formation during heart development (Figure 3). By E14.5, the entire dorsal heart surface is covered by a hierarchical coronary vasculature in control A^{flox}/A^{flox} littermates (Figure 3a); the coronary vasculature fails to cover the apex area in A^{Tie2}/A^{Tie2} hearts (Figure 3c). Despite a very limited avascular area at the apex, B^{Tie2}/B^{Tie2} hearts have no major defect in the coronary vasculature (Figure 3b). However $A^{+}/A^{Tie2}; B^{Tie2}/B^{Tie2}$ hearts show a major reduction of coronary coverage (Figure 3d) which is even more severe than that seen in A^{Tie2}/A^{Tie2} hearts. Avascular areas were measured

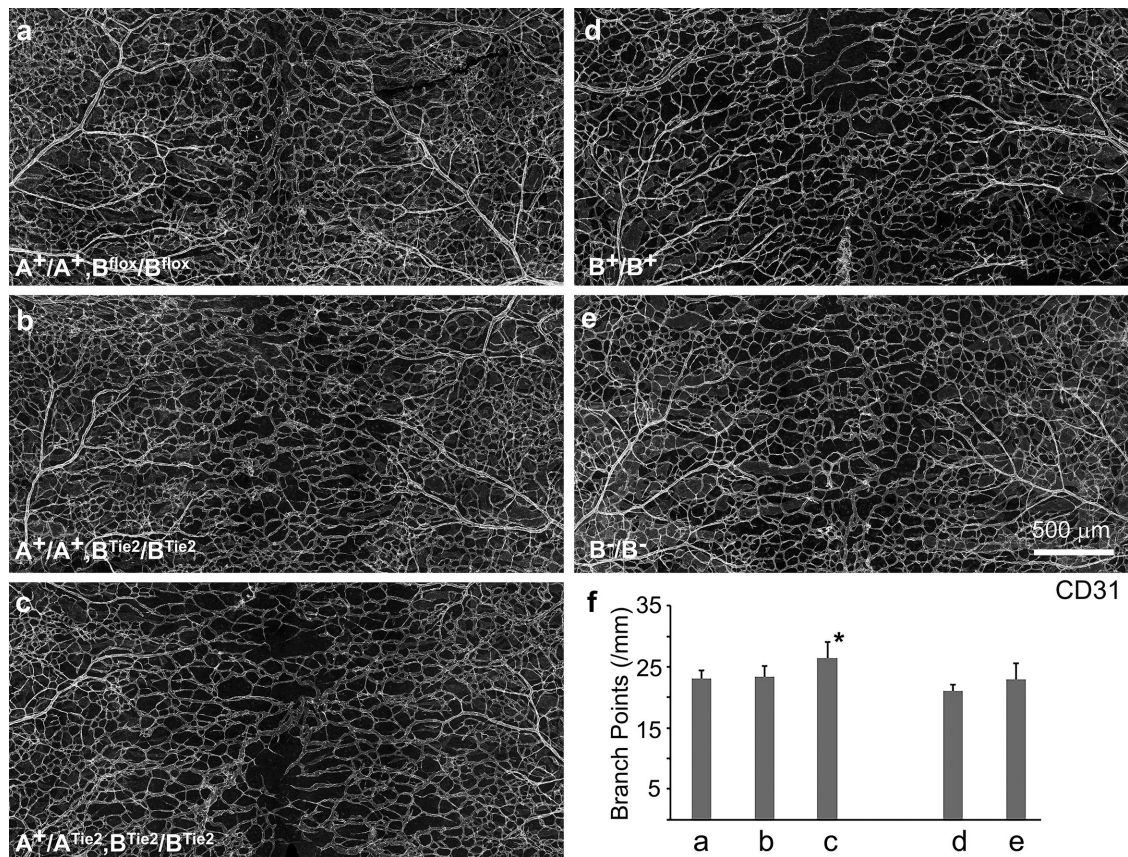


FIGURE 2: Ablation of NM2B impairs blood vessel formation when NM2A is not fully expressed. Wholemount confocal images of mouse back skins at E14.5 from various genotypes (as indicated) stained with CD31 antibodies show that mice ablated for NM2B in endothelial cells (b, $A^+/A^+; B^{Tie2}/B^{Tie2}$) or in the germline (e, B^-/B^-) have no defects in blood vessel formation as compared with their control littermates $A^+/A^+; B^{flox}/B^{flox}$ (a) and B^+/B^+ (d), respectively. Ablation of one copy of NM2A in B^{Tie2}/B^{Tie2} mice (c, $A^+/A^{Tie2}; B^{Tie2}/B^{Tie2}$) results in immature back skin blood vessels together with moderately reduced blood vessel coverage compared with the control littermate, a. Panel f quantifies average branch points of vascular networks for each genotype. Bars a to e correspond to panels a to e, respectively. $A^+/A^{Tie2}; B^{Tie2}/B^{Tie2}$ vasculature, c, shows a moderate increase in branch points (27 ± 3 , $n = 4$, $p < 0.05$) from control $A^+/A^+; B^{flox}/B^{flox}$ mice, a (23 ± 1 , $n = 4$). * $p < 0.05$ (one way ANOVA, Post Turkey).

using ImageJ (Figure 3e). The average percentages of the avascular area over the entire dorsal heart surface are $2 \pm 2\%$, $4 \pm 3\%$, $19 \pm 3\%$, and $30 \pm 8\%$ for A^{flox}/A^{flox} , B^{Tie2}/B^{Tie2} , A^{Tie2}/A^{Tie2} , and $A^+/A^{Tie2}; B^{Tie2}/B^{Tie2}$ hearts, respectively ($n = 3$ for each genotype, $p < 0.05$ between two of each groups by one way ANOVA, Post Turkey). In addition, coronary vasculature in both A^{Tie2}/A^{Tie2} (c) and $A^+/A^{Tie2}; B^{Tie2}/B^{Tie2}$ (d) hearts appears immature compared with control and B^{Tie2}/B^{Tie2} hearts (a, b). These results indicate that coronary vascular formation relies more on the function of NM2B compared with skin vascular formation. Again, we find no changes in vascular patterning in the developing coronary vessels with various combinations of NM2A and 2B ablation.

To further demonstrate the importance of NM2B in vascular network formation during embryonic development, we ablated NM2A and 2B together in mice using crosses to an inducible VE-cadherin-Cre mouse ($Cdh5-CreER$). Introduction of tamoxifen at E10.5 circumvents the early embryonic lethality found in $Tie2$ -cre-mediated NM2A and 2B doubly ablated mice. Crossing $A^+/A^{Cdh5}; B^+/B^{Cdh5}$ males with $A^{flox}/A^{flox}; B^{flox}/B^{flox}$ females generates various combinations of $Cdh5-CreER$ -mediated NM2A and NM2B compound ablated mice. Supplemental Figure S4 demonstrates the efficiency of NM2 ablation from these crossing. Figure 4, a–d displays embryos

of littermates at E13.5 following a single intraperitoneal injection of tamoxifen at E10.5. $A^+/A^{Cdh5}; B^{Cdh5}/B^{Cdh5}$ mice, which express one copy of NM2A and no 2B, show no obvious abnormalities, in contrast to $A^{flox}/A^{flox}; B^{flox}/B^{flox}$ control littermates (Figure 4, a and b). $A^{Cdh5}/A^{Cdh5}; B^+/B^{Cdh5}$ mice, which express one copy of NM2B and no 2A, develop obvious hemorrhages (Figure 4c, yellow arrows). $A^{Cdh5}/A^{Cdh5}; B^{Cdh5}/B^{Cdh5}$ mice, which express no NM2A and no 2B, develop severe hemorrhages (Figure 4d, yellow arrows). Thus both NM2A and 2B are functioning to maintain the integrity of blood vessels during mouse embryonic development. A similar graded severity of vascular network defects in the back skin is observed among these genotypes (Figure 4, e–h). Compared with that in the control floxed littermates (Figure 4e), the vascular network in the back skin of $A^+/A^{Cdh5}; B^{Cdh5}/B^{Cdh5}$ mice appears normal (Figure 4f). $A^{Cdh5}/A^{Cdh5}; B^+/B^{Cdh5}$ back skin shows obvious abnormalities in vascular network formation and coverage (Figure 4g), and $A^{Cdh5}/A^{Cdh5}; B^{Cdh5}/B^{Cdh5}$ back skin shows the most severe defects (Figure 4h). The average branch points per millimeter length are 24 ± 3 ($n = 5$) for controls, 25 ± 1 ($n = 5$) for $A^+/A^{Cdh5}; B^{Cdh5}/B^{Cdh5}$ mice, 33 ± 2 ($n = 5$) for $A^{Cdh5}/A^{Cdh5}; B^+/B^{Cdh5}$ mice, and 66 ± 4 ($n = 5$) for $A^{Cdh5}/A^{Cdh5}; B^{Cdh5}/B^{Cdh5}$ mice (Figure 4i). Both $A^{Cdh5}/A^{Cdh5}; B^+/B^{Cdh5}$ and $A^{Cdh5}/A^{Cdh5}; B^{Cdh5}/B^{Cdh5}$ mice show significant increases in vascular branch points as

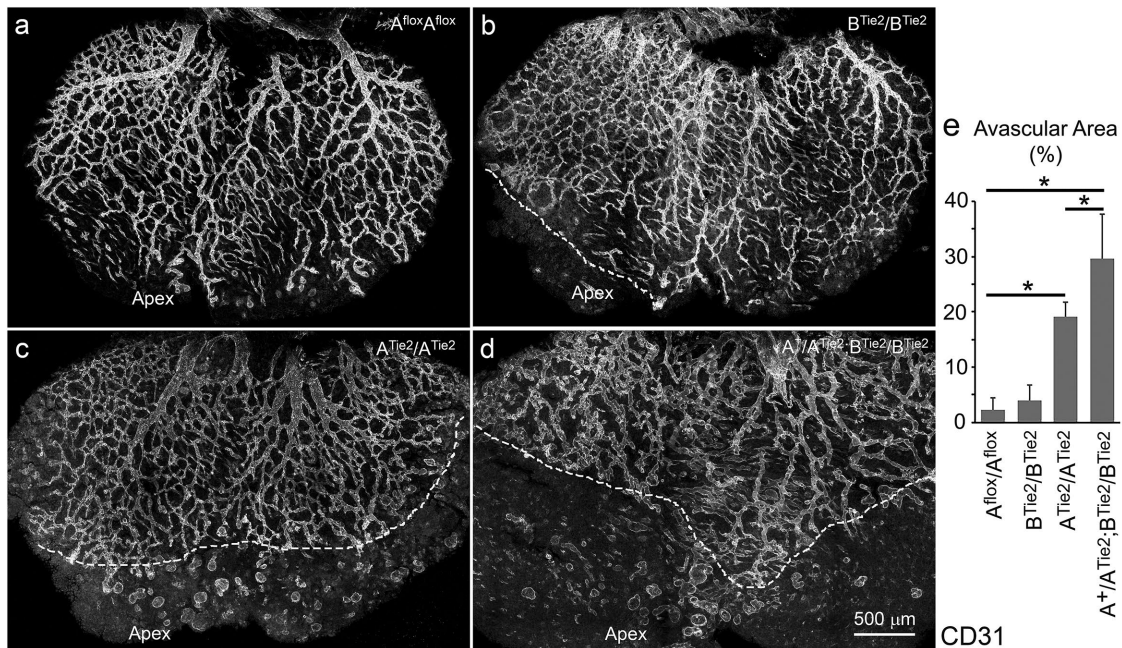


FIGURE 3: Abnormal coronary vessel formation in endothelial specific NM2-ablated mouse hearts. Wholemount confocal images of coronary vessels in the dorsal surface of E14.5 mouse heart stained with CD31 antibodies show that the coronary vasculature completely covers the entire dorsal surface in control cre-negative mice (a). B^{Tie2}/B^{Tie2} hearts have a minor defect in coronary vasculature (b) compared with control hearts (a). A^{Tie2}/A^{Tie2} hearts lack coronary vasculature covering the apex of the hearts (c). A⁺/A^{Tie2}; B^{Tie2}/B^{Tie2} hearts show a marked reduction in coronary coverage (d). Dashed white lines in panels b, c, and d depict the front of vascular sprouts in mutant hearts. Panel e quantifies avascular areas for each genotype. *n* = 3 for each genotype. **p* < 0.05 between two groups (one-way ANOVA, post Tukey).

compared with the control mice (*p* < 0.01, one-way ANOVA). Moreover, branch points in A^{Cdh5}/A^{Cdh5}; B^{Cdh5}/B^{Cdh5} mice are also significantly more numerous than those in A^{Cdh5}/A^{Cdh5}; B⁺/B^{Cdh5} mice (*p* < 0.01). Thus, NM2B is important when the expression of NM2A is not sufficient (heterozygous and homozygous) during vascular network formation. Importantly, when only a single allele of NM2A is expressed, the expression of NM2B is essential and sufficient to support normal development of blood vessels in mice. All these results further support the role of NM2 in the prevention of vascular over-branching during embryonic development.

We have previously demonstrated that mice expressing NM2B or NM2C in place of NM2A under the control of the endogenous Myh9 promoter die early by E9.5 or E10.5, respectively, with abnormalities in blood vessel formation (Wang *et al.*, 2010; Zhang *et al.*, 2018). Therefore, the total amount of NM2 is not the single most important factor in blood vessel formation.

Loss of NM2A causes excessive branching in embryoid body sprouting angiogenesis

As shown above, ablation of NM2 expression from endothelial cells in mice resulted in an increased branching morphogenesis during embryonic vascular network formation. Because NM2A plays the major role, we next focused on the role of NM2A in 3D sprouting angiogenesis. We employed an *in vitro* 3D sprouting angiogenesis assay using embryoid bodies (EBs) generated from wild-type (A⁺/A⁺) and NM2-ablated (A⁻/A⁻) mouse embryonic stem cells. A⁻/A⁻ embryonic stem cells were generated by homologous recombination as previously described (Conti *et al.*, 2004). A⁺/A⁺ and A⁻/A⁻ EBs were embedded and cultured side by side in pairs in a 1.5-mg/ml collagen gel containing 30 ng/ml VEGF-A. Immunofluorescence staining of EB sprouts with antibodies against the heavy chain of

NM2A (NMHC2A) confirms the ablation of NM2A in A⁻/A⁻ EBs (Supplemental Figure S5, c and d). NM2A is detected in A⁺/A⁺ EBs (Supplemental Figure S5, a and b). Figure 5A shows the endothelial sprouts stained with the CD31 antibody following 7 d in culture. A⁺/A⁺ sprouts in general appear straight and smooth (left, magnified below), A⁻/A⁻ sprouts are much thinner with a marked increase in branches (right, magnified below). We quantified the density of the branching points and measured the length of the branches from cultured EB sprouts using the AngioTool (Figure 5C). The density of branch points is significantly higher in A⁻/A⁻ sprouts (10 ± 3 per millimeter of sprout, *n* = 32) than in the control A⁺/A⁺ sprouts (5 ± 2 per millimeter of sprout, *n* = 44, *p* < 0.0001). Correspondingly, A⁻/A⁻ sprouts show a marked decrease in average length of the branch (0.86 ± 0.26 mm, *n* = 32) compared with A⁺/A⁺ sprouts (1.26 ± 0.82 mm, *n* = 44, *p* < 0.05). Figure 5B shows phase-contrast images of the sprouts. Compared with the wild-type sprouts (Figure 5B, a and b), A⁻/A⁻ sprouts develop excessive branches and cortical protrusions (Figure 5B, c and d, arrows). Panels b and d are enlarged from the boxed areas of panels a and c, respectively. Time-lapse videos of growing sprouts further reveal that in A⁺/A⁺ growing sprouts, the endothelial cells migrate collectively, and the tip of the sprout develops one dominant protrusion that leads to a persistent growth of sprouts (Supplemental Movie S1a). A⁻/A⁻ sprouts, however, often develop multiple protrusions at the tip causing frequent splitting and/or turning of the sprouts (Supplemental Movie S1b). Together, these results demonstrate that loss of NM2A results in an increase in vascular branching during sprouting angiogenesis due to a defect in persistent sprouting. To further confirm these results, a second line of NM2A ablated mouse embryonic stem cells was generated using CRISPR and the 3D sprouting angiogenesis studies were repeated. Supplemental Figure S5, e and f demonstrates the ablation of

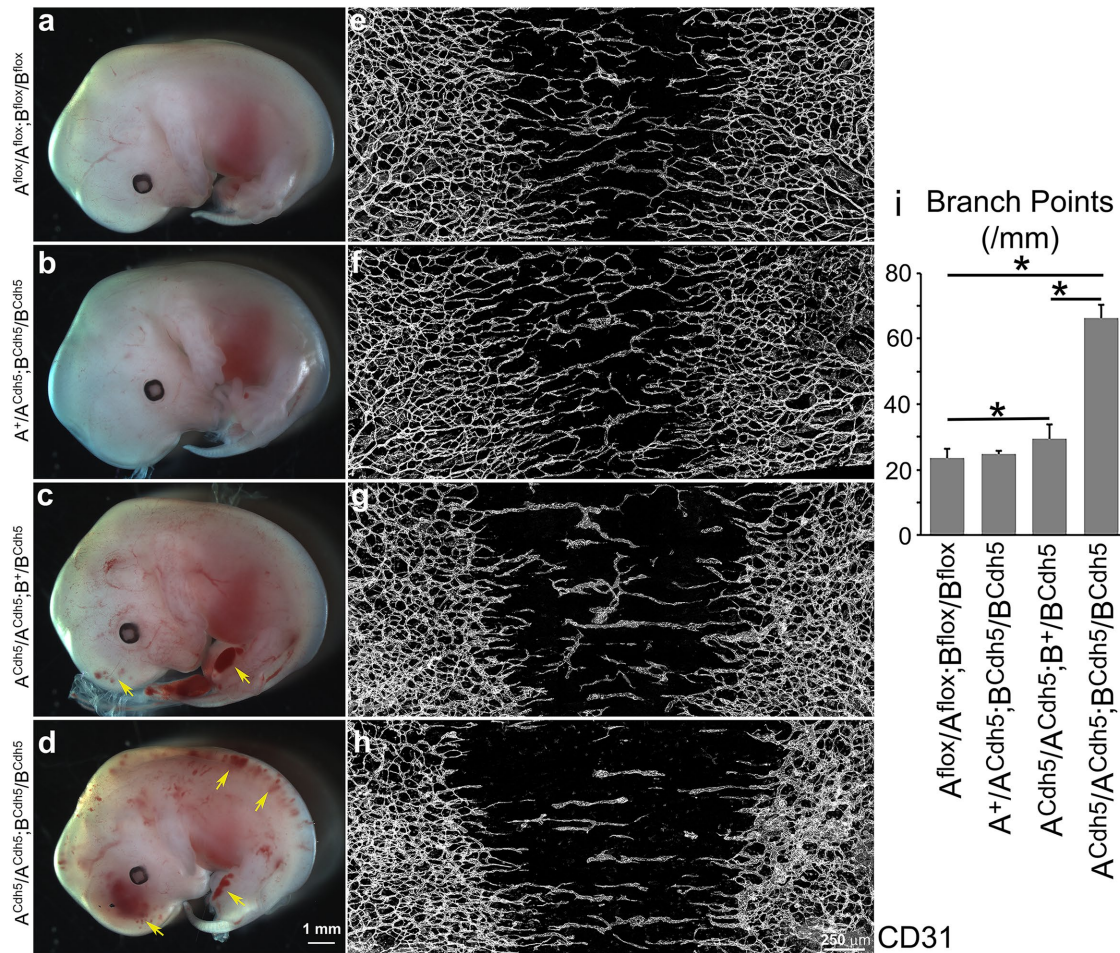


FIGURE 4: NM2B is essential for endothelial cells when NM2A is not expressed. (a–d) Images of E13.5 mouse embryos with various combinations of tamoxifen-induced (injection at E10.5) NM2A and 2B ablation after crosses with Cdh5–CreER mice show that with total ablation of NM2A from endothelial cells, an additional ablation of one copy of NM2B results in minor hemorrhages in A^{Cdh5}/A^{Cdh5}; B⁺/B^{Cdh5} mice, c. Complete ablation of NM2A and 2B together leads to severe hemorrhages in A^{Cdh5}/A^{Cdh5}; B^{Cdh5}/B^{Cdh5} mice, d. Mice ablated for one copy of NM2A together with both copies of NM2B, b (A⁺/A^{Cdh5}; B^{Cdh5}/B^{Cdh5}) do not show obvious abnormalities compared with control mice, a. (e–h) Wholemount confocal images of back skin vasculature from mouse embryos described above, a–d, show that with total ablation of NM2A from endothelial cells, additional ablation of one copy of NM2B results in reduced coverage of vasculature in A^{Cdh5}/A^{Cdh5}; B⁺/B^{Cdh5} mice, g. Ablation of both copies of 2B causes a severe decrease in vascular coverage in A^{Cdh5}/A^{Cdh5}; B^{Cdh5}/B^{Cdh5} mice, h. Mice ablated for one copy of NM2A together with both copies of NM2B, f (A⁺/A^{Cdh5}; B^{Cdh5}/B^{Cdh5}) show no defect in blood vessels compared with control mice, a. Panel i quantifies average branch points for each genotype. *n* = 5 for each genotype. **p* < 0.01 between two groups (one-way ANOVA, post Tukey).

NM2A in CRISPR A⁻/A⁻ sprouts. Again, CRISPR-NM2A–ablated EBs show excessive vascular branching (Supplemental Figure S6b) as compared with the isogenic wild-type EBs (Supplemental Figure S6a). The average branch points of CRISPR A⁻/A⁻ sprouts (10 ± 1 per mm sprouts, *n* = 5, *p* < 0.01) are significantly more numerous than those of the wild-type sprouts (4 ± 2 per mm sprouts, *n* = 6; Supplemental Figure S6d). Using CRISPR, we also generated NM2B–ablated mouse embryonic stem cells. Supplemental Figure S5, g–j confirms the ablation of NM2B expression in CRISPR B⁻/B⁻ sprouts (i, j). NM2B is detected in wild-type (B⁺/B⁺) sprouts (g, h). Ablation of NM2B does not affect EB sprouting angiogenesis (Supplemental Figure S6c; Supplemental Movie S1c). The average number of branch points of CRISPR B⁻/B⁻ sprouts is 4 ± 2 per mm of sprout (*n* = 5), which is no different from that for the wild-type sprouts (Supplemental Figure S6d). These results are consistent with our findings from NM2 conditionally ablated mice, suggesting that defects of blood vessel formation in NM2 conditionally ablated mice

are primarily due to the loss of NM2 function during sprouting angiogenesis.

Loss of cortical stability in NM2A–ablated vascular sprouts

To understand how ablation of NM2A causes overbranching during sprouting angiogenesis, time-lapse videos of EB sprouting were captured at a frequency of 1 s per frame and carefully analyzed for the behavior of the sprouts. In A⁺/A⁺ EBs, the front of growing sprouts generates numerous cortical blebs with an average lifetime of 15 ± 3 s (*n* = 50, Supplemental Movie S2a, arrow). Typical blebbing consists of a fast phase of protrusion and growth followed by a slower phase of retraction (Supplemental Figure S7a, Front; enlarged in panel S7d). Blebs quickly form at the front of the sprouts following the protrusion of the tip cells. Blebs are also observed at the back of the sprouts but with decreased frequency (Supplemental Figure S7a, Back). In contrast, the front of A⁻/A⁻ sprouts show no dynamic blebbing but develop marked cortical ruffles with multiple

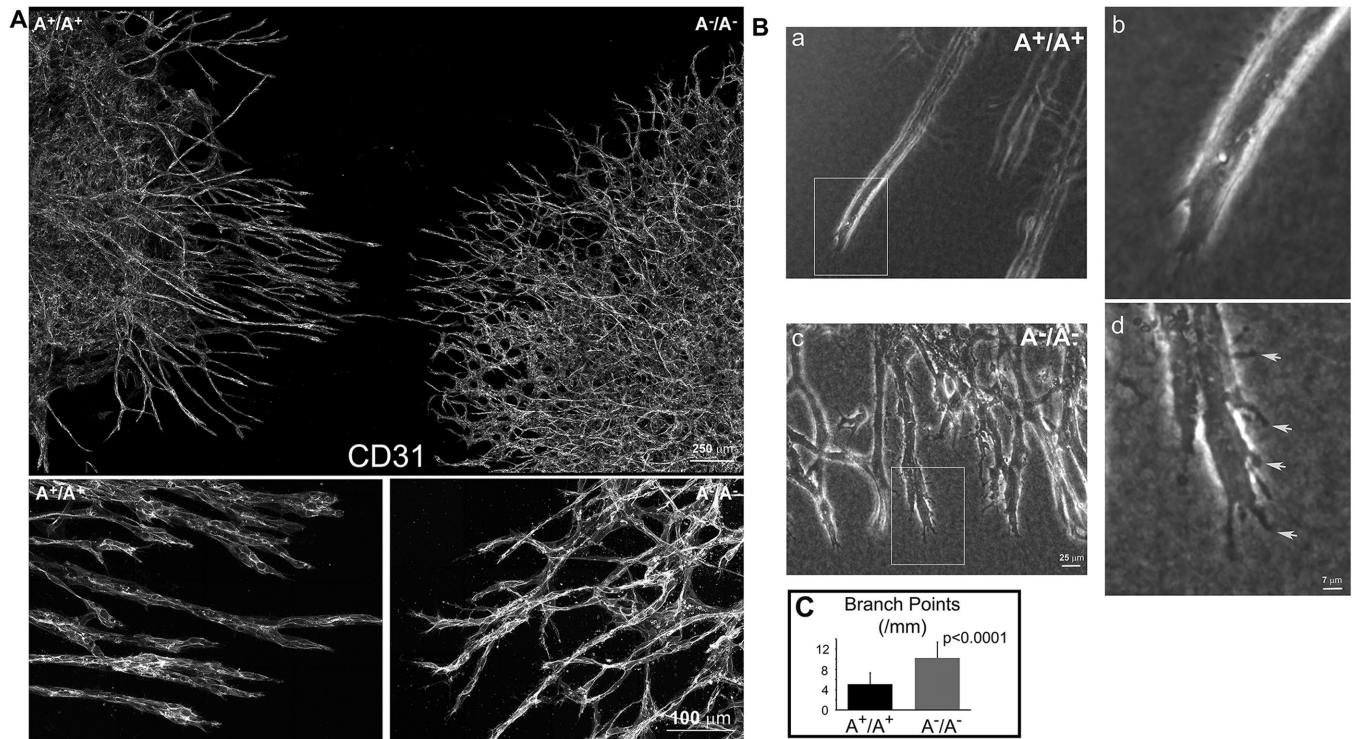


FIGURE 5: Excessive branching of A^{-}/A^{-} angiogenic sprouts from EBs cultured in 3D collagen. (A) Z-projections of confocal images from A^{+}/A^{+} and A^{-}/A^{-} angiogenic sprouts stained with CD31 antibodies for endothelial cells show that A^{-}/A^{-} sprouts (Right) develop more branches than A^{+}/A^{+} sprouts (Left). The average densities of branch points are 10 ± 3 ($n = 32$) and 5 ± 2 ($n = 44$) per millimeter of sprout for A^{-}/A^{-} and A^{+}/A^{+} sprouts, respectively ($p < 0.0001$). The average lengths of branches are 0.86 ± 0.26 mm ($n = 32$) and 1.26 ± 0.82 mm ($n = 44$) for A^{-}/A^{-} and A^{+}/A^{+} sprouts, respectively ($p < 0.05$). The panels at the bottom show a magnified view of the upper panel. (B) Phase contrast images of A^{+}/A^{+} (a, magnified in b) and A^{-}/A^{-} (c, magnified in d) angiogenic sprouts show that A^{+}/A^{+} sprouts in general are straight and smooth, b, while A^{-}/A^{-} sprouts have excessive branches and cortical protrusions—d, arrows. (C) Quantification of average branch points for A^{+}/A^{+} ($n = 44$) and A^{-}/A^{-} ($n = 32$) sprouts. $p < 0.0001$.

protrusions (Supplemental Movie S2b, arrow). Instead of blebbing, the backs of A^{-}/A^{-} sprouts show slow cortical fluctuations (Supplemental Figure S7b, Back), suggesting a reduction of cortical tension compared with that in the wild-type sprouts. Interestingly, cortical blebbing requires NM2A but not NM2B. NM2B-ablated sprouts show normal sprouting and blebbing similar to those in the wild-type sprouts (Supplemental Movie S1c; Supplemental Movie S2c, arrow; Supplemental Figure S7c). The actomyosin cytoskeletons in A^{-}/A^{-} and A^{+}/A^{+} sprouts were examined by staining with antibody to CD31 and Alexa-488 phalloidin for F-actin. A^{+}/A^{+} sprouts are generally encircled by thick actomyosin bundles around the entire sprout, manifesting a mechanically coupled migratory unit, and they develop numerous filopodia-like structures that are enriched at the tips of the sprouts during navigation (Figure 6a). The stress fibers in A^{+}/A^{+} sprouts align along the long axis of the sprouts (Figure 6a, enlarged in c, green). In contrast, A^{-}/A^{-} sprouts are not as compact, show no obvious boundary of actin bundles surrounding the sprouts, and show a marked reduction in filopodia formation and stress fibers (Figure 6b, enlarged in d, green). Instead of filopodia-like structures, A^{-}/A^{-} sprouts develop numerous balloon-like protrusions (Figure 6d, arrows) reminiscent of membrane ruffles in cells under 2D culture. We counted the filopodia numbers at the tip of the sprouts and measured the lengths of the filopodia using ImageJ (Figure 6, e and f). The average numbers of filopodia per sprout for A^{+}/A^{+} and A^{-}/A^{-} sprouts are respectively 8 ± 3 ($n = 21$) and 3 ± 1 ($n = 28$; $p < 0.0001$). The average lengths of filopodia for A^{+}/A^{+} ($n = 103$) and A^{-}/A^{-} ($n = 115$) sprouts are

7.6 ± 3.1 μ m and 4.5 ± 2.0 μ m, respectively ($p < 0.0001$). These results suggest that loss of NM2A impairs the cortical membrane stability in sprouts. Fibroblast cells lacking NM2 function develop excessive lamellipodia ruffling associated with impaired focal adhesion maturation when cultured on a flat surface (Lo *et al.*, 2004; Even-Ram *et al.*, 2007; Ma *et al.*, 2017). Focal adhesions in EB sprouts were examined by staining for phosphopaxillin (pPaxillin, a marker of mature focal adhesions). Figure 7 shows that mature focal adhesions in A^{+}/A^{+} sprouts align parallel to the long axis of the sprouts (Figure 7a, enlarged in b, green), similarly to the focal adhesions seen in mesenchymal cells cultured in a 3D matrix (Cukierman *et al.*, 2001). In A^{-}/A^{-} sprouts, however, pPaxillin signaling is markedly reduced and shows no regularity in alignment (Figure 7c, enlarged in d, green). The fluorescence intensity of pPaxillin staining was quantified using ImageJ (Figure 7g). The relative fluorescence intensity (arbitrary units) of A^{+}/A^{+} sprouts is 132 ± 28 ($n = 60$), which is significantly greater than for A^{-}/A^{-} sprouts, for which it is 9 ± 5 ($n = 48$, $p < 0.0001$). The alignment of adhesion was analyzed using ImageJ Directionality. A^{+}/A^{+} sprouts show an obvious peak corresponding to their major alignment along the long axis of the sprouts (Figure 7e), while the peak in A^{-}/A^{-} sprouts is markedly damped (Figure 7f). Accordingly, the Dispersion index (Figure 7h; a measurement of deviation from the Directionality analysis) is significantly larger for A^{-}/A^{-} sprouts ($28 \pm 14^{\circ}$, $n = 11$, $p < 0.01$) than for A^{+}/A^{+} sprouts ($13 \pm 4^{\circ}$, $n = 10$). Thus, NM2A plays an important role in maintaining cortical integrity and in the regulation of focal adhesions during sprouting angiogenesis.

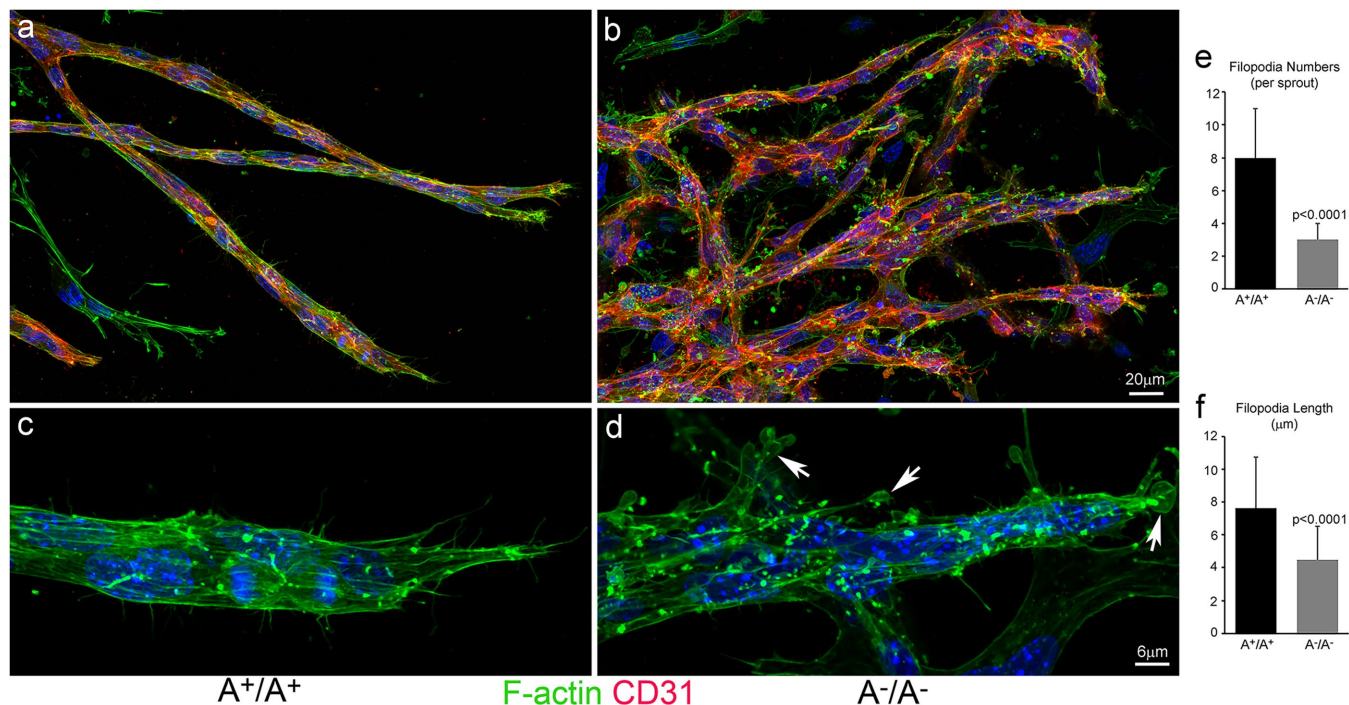


FIGURE 6: Abnormal actin organization in A⁻/A⁻ angiogenic sprouts. Confocal images of A⁺/A⁺ (a) and A⁻/A⁻ (b) angiogenic sprouts stained with CD31 (red) and Alexa488-phalloidin for F-actin (green) show disruption of stress-fibers in A⁻/A⁻ sprouts (b, magnified in d) compared with A⁺/A⁺ sprouts (a, magnified in c). The stress fibers are aligned along the long axis in A⁺/A⁺ sprouts. A⁻/A⁻ sprouts show a great reduction in stress-fibers and develop numerous balloonlike cortical membrane protrusions manifesting membrane ruffling—d, arrows. Panel e quantifies the average numbers of filopodia at the tip of sprouts ($n = 21$ and 23 for A⁺/A⁺ and A⁻/A⁻ sprouts, respectively, $p < 0.0001$). Panel f quantifies the average length of filopodia ($n = 103$ and 115 for A⁺/A⁺ and A⁻/A⁻ sprouts, respectively, $p < 0.0001$).

NM2A dynamics during cortical protrusion and retraction during EB sprouting were investigated next. Using EGFP-NM2A embryonic stem cells (where EGFP is fused to the N-terminal of the endogenous nonmuscle myosin heavy chain 2A), we recorded time-lapse videos of EGFP-NM2A signals during EB sprouting. As shown in Supplemental Movie S3, the cortical protrusions initiate at an area with reduced NM2A signal; however, an increase of NM2A intensity is observed during cortical retraction. Figure 8Ab shows the kymograph of EGFP-NM2A dynamics along the line shown in Figure 8Aa. The relative NM2A intensity is shown in a “Fire” scale to better visualize the differences. NM2A intensity increases during retraction from a low “blue” to a high “orange” in all four retraction events (Figure 8Ab, arrows). Figure 8B, a–c shows a timed series of images at 5, 10 and 15 s of a single retraction, which further demonstrates increased NM2A intensity during cortical retraction. EGFP-NM2A fluorescence intensity (au, arbitrary units) was quantified using ImageJ (Figure 8Bd). The average EGFP-NM2A intensities ($n = 10$ events) are 62 ± 18 , 84 ± 14 , and 119 ± 28 au, respectively. All these results are consistent with the role of NM2A in cortical retraction. Actomyosin therefore provides the mechanical machinery that is required for maintaining cortical stability and prevents excessive protrusion during sprouting angiogenesis.

ROCK-activated NM2A activity is required during sprouting angiogenesis

To further confirm that sprouting angiogenesis requires NM2 enzymatic ATPase activity, we introduced the myosin inhibitor blebbistatin into the EB sprouting assay. Blebbistatin inhibits NM2 MgATPase activity by blocking phosphate release from ADP. Movie Supplemental S4a shows that the application of 10 μ M blebbistatin

results in excessive branching. The sprouts develop multiple protrusions and no dynamic cortical blebbing, which phenocopies the abnormalities of the NM2A ablated sprouts. We next examined the upstream activator of NM2 during angiogenesis. NM2 myosin MgATPase activity is activated by two major kinases, Rho kinase and Ca-calmodulin-dependent myosin-light chain kinase, which phosphorylate the regulatory myosin light chain. Inhibition of Rho kinase by Y27632 (10 μ M) results in abnormal branching and the loss of cortical blebbing, similarly to blebbistatin inhibition of NM2 activity (Supplemental Movie S4b). However, inhibition of myosin-light chain kinase by ML-7 (20 μ M) has no effect on sprouting (Supplemental Movie S4c). Applications of blebbistatin (10 μ M) and Y27632 (10 μ M), but not ML-7 (20 μ M), during EB-sprouting angiogenesis assays overnight at day 6 significantly increases sprout branching morphogenesis (Supplemental Figure S8). The average branch points of blebbistatin- and Y27632-treated sprouts are 7 ± 2 ($n = 14$) and 7 ± 1 ($n = 14$), respectively; those are significantly more numerous than those of the sprouts treated with the same amount of solvent DMSO (4 ± 2 , $n = 14$, $p < 0.01$). ML-7 does not increase the branch points of the sprouts (5 ± 1 , $n = 9$). Supplemental Figure S8e shows the quantification of the average branch points. All of these results demonstrate that Rho kinase-activated NM2 activity is essential for sprouting angiogenesis.

We next asked whether Rho kinase-activated NM2 was important in embryonic vascular development in vivo. There are many reports supporting the role of Rho kinase in the regulation of vascular network formation (Bryan *et al.*, 2010; Kamijo *et al.*, 2011; Liu *et al.*, 2018). The importance of Rho kinase in vascular formation, however, is not well demonstrated during embryonic development in vivo. Two Rho kinases (ROCK1 and ROCK2) are expressed in

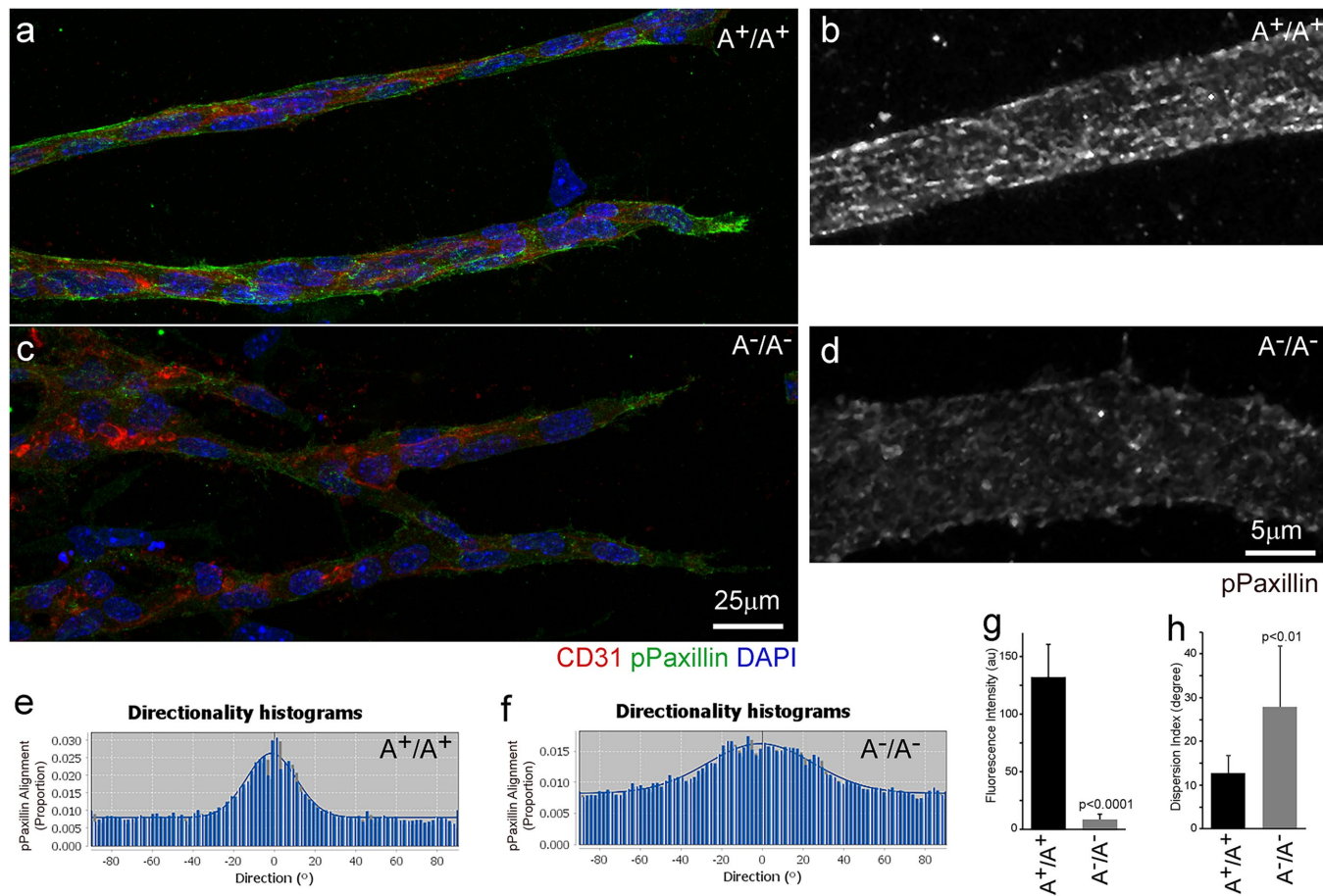


FIGURE 7: Defects in focal adhesion formation in A^{-}/A^{-} angiogenic sprouts. (a–d) Confocal images of angiogenic sprouts stained with antibodies for phosphopaxillin (green, a marker for mature focal adhesions) and CD31 (red, a marker for endothelial cells) show that A^{+}/A^{+} sprouts develop mature focal adhesions that align in parallel along the long axis of sprouts (a, magnified in b, green). Mature focal adhesions are infrequently observed in A^{-}/A^{-} sprouts and they are randomly distributed (c, magnified in d, green). (e, f) Representative directionality histograms of phosphopaxillin staining in A^{+}/A^{+} and A^{-}/A^{-} sprouts obtained from the Directional analysis. A^{+}/A^{+} sprouts show an obvious peak (e), which is consistent with a major alignment of focal adhesions along the long axis of the sprouts. A^{-}/A^{-} sprouts show a markedly damped peak (f) reflecting a loss of alignment. Panel g quantifies the average fluorescence intensity of pPaxillin staining ($n = 60$ and 48 for A^{+}/A^{+} and A^{-}/A^{-} sprouts, respectively, $p < 0.0001$). Panel h quantifies the average dispersion index (a measurement of deviation from the Directionality analysis) of pPaxillin alignments ($n = 10$ and 11 for A^{+}/A^{+} and A^{-}/A^{-} sprouts, respectively, $p < 0.01$).

endothelial cells and show overlapping roles during embryonic mouse development. The small GTPase RhoA is the major upstream activator of the Rho kinases. We therefore next ablated RhoA in mouse endothelial cells using $Cdh5$ -CreER mice and examined the skin and cardiac vascular development in these mice. Figure 9 shows E15.5 mouse embryos following a tamoxifen injection at E10.5 to induce RhoA ablation. Embryos ablated for RhoA develop edema and hemorrhage (Figure 9b). Compared with the control mice (Figure 9c, $RhoA^{fllox}/RhoA^{fllox}$), mice ablated for RhoA in endothelial cells do not show obvious defects in the coverage of blood vessels and branching morphogenesis in the back skin at E15.5 (Figure 9d, $RhoA^{Cdh5}/RhoA^{Cdh5}$). The average branch points for $RhoA^{fllox}/RhoA^{fllox}$ and $RhoA^{Cdh5}/RhoA^{Cdh5}$ back skin vasculatures are 28 ± 3 and 29 ± 1 per mm length, respectively ($n = 4$ each, $p = 0.13$, Figure 9g). The maturation of the vasculature, however, is delayed in $RhoA^{Cdh5}/RhoA^{Cdh5}$ back skin, which shows no remodeled blood vessels in the middle of the back (Figure 9d). These mature vessels are evident in the control littermate (Figure 9c, arrows). Interestingly, coronary vessel development in RhoA ablated mice is severely

impaired, showing a marked reduction of coronary vessel coverage at the apex of the dorsal surface of the heart (Figure 9f, below the dashed line) compared with that in control mice, where the coronary vasculature completely covers the dorsal surface of the heart ventricle (Figure 9e). The average percentage of the avascular area for $RhoA^{Cdh5}/RhoA^{Cdh5}$ hearts is $43 \pm 7\%$ ($n = 3$, Figure 9h). There is no avascular area for $RhoA^{fllox}/RhoA^{fllox}$ hearts. These results suggest that RhoA/RhoA activated kinase activation of NM2A plays an important role in blood vessel development in vivo, especially during mouse cardiac coronary vessel formation.

In summary, we show that NM2A plays a major role in persistent vascular sprouting and that NM2A functions to prevent excessive branching from sprouts by maintaining cortical stability through focal adhesions and facilitation of cortical membrane retraction.

DISCUSSION

Our results from singly NM2A or NM2B endothelial cell-ablated mice and 3D EB angiogenic sprouting show that NM2A, but not NM2B, is required for sprouting angiogenesis. Similar findings are

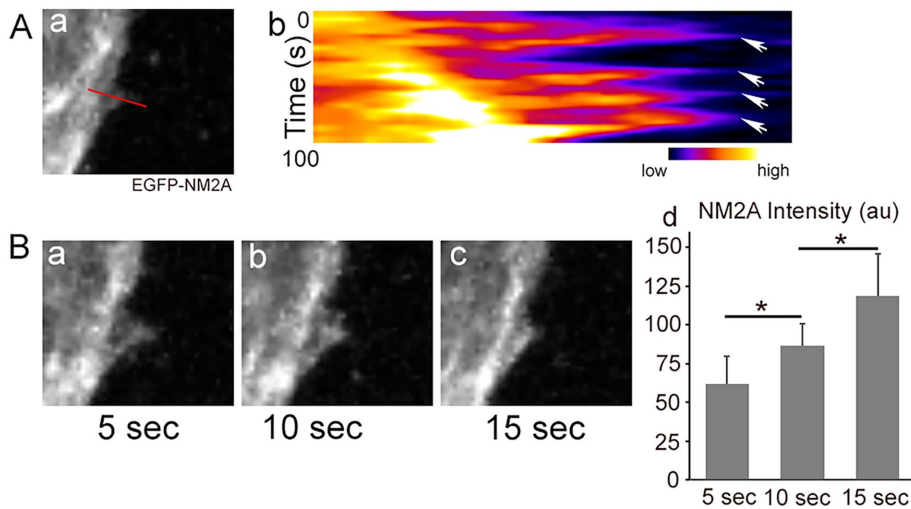


FIGURE 8: Increase of NM2A intensity during cortical retraction in angiogenic EB sprouting. (A) Kymograph of NM2A dynamics (b) along the line indicated in panel a during angiogenic EB sprouting. NM2A intensity is shown in a “Fire” scale. NM2A intensity increases from a low “blue” to a high “orange” in all four retraction events—b, arrows. (B) A time series of a retraction event (a–c) demonstrates a gradual increase of NM2A from panel a to panel c during cortical retraction. NM2A intensity is lowest in panel a and highest in panel c among the three time points. Panel Bd quantifies the average EGFP–NM2A fluorescence intensity (au, arbitrary units). $n = 10$, $*p < 0.05$ between two groups (one-way ANOVA, post Tukey). Note that the sprout shows a general shift from left to right during imaging as shown both from the kymograph, A, and the time series, B.

reported for a 3D biomimetic model of angiogenesis using HUVECs by CRISPR ablation of NM2A and 2B individually (Yoon *et al.*, 2019). Our analyses of endothelial NM2A and 2B compound ablated mice further show that NM2B also plays important roles in angiogenesis. Together with NM2A ablation, ablation of NM2B potentiates blood vessel abnormalities in mice, including a further decrease of blood vessel coverage and an increase of hemorrhage in mutant embryos. One possible explanation is that NM2A and 2B compensate for each other when one paralog is missing. A second possible explanation is that NM2A and 2B complement each other in regulating angiogenesis. Previously, results from NM2 paralog genetic swapping studies demonstrated that NM2A is uniquely required for placental vascular development in mice, which is not consistent with compensation between NM2A and 2B (Wang *et al.*, 2010; Zhang *et al.*, 2018). Our results here favor the notion that NM2A and 2B function complementarily in regulation of angiogenesis. Dynamic regulation of endothelial cell–cell adhesion plays key roles for angiogenic sprouting activity (Szyborska and Gerhardt, 2018). Weakening of cell–cell adhesion promotes sprouting. NM2 activity is required for filopodia-like bridge formation and recruitment of VE–cadherin in nascent adherens junctions in cultured endothelial cells (Liu *et al.*, 2010; Hoelzle and Svitkina, 2012). In cultured epithelial MDCK cells, NM2A and NM2B have been shown to function complementarily in the formation and maintenance of the integrity of adherens junctions (Heuze *et al.*, 2019). During adherens junction formation, NM2A and 2B are differentially localized to and stabilize the perijunctional contractile actin bundles and the juxtamembrane actin meshwork, respectively. NM2A provides the major tugging force for junction growth, while NM2B is required for E-cadherin clustering and coupling of perijunctional contractile actin to the plasma membrane, and provides the majority of intercellular stress (Heuze *et al.*, 2019). In mature adherens junctions, junctional localization of NM2A and 2B is also differentially regulated. Rho/ROCK

and myosin–light chain kinase activity are required for NM2A localization, whereas junctional NM2B depends on Rap1 (Smutny *et al.*, 2010). All these findings support the idea that NM2A and 2B function complementarily but in different aspects of cell–cell adhesions. However, we failed to detect obvious abnormalities in NM2B endothelial cell–ablated mice and in NM2B-ablated sprouting angiogenesis in vitro using EBs.

NM2 promotes cortical protrusion retraction ensuring processive sprouting and preventing excessive branching. The back skin vasculature in mice ablated for NM2A develops increased branching morphogenesis. NM2A null endothelial sprouts from an in vitro angiogenic sprouting assay also show increased branching activity. Thus NM2 is important to inhibit excessive branching during angiogenic sprouting. This is consistent with the findings that inhibition of Rho kinase activity increases sprouting activity (Abraham *et al.*, 2009; Kroll *et al.*, 2009). This is also supported by the report that inhibition of NM2 activity by either the myosin inhibitor blebbistatin or the Rho kinase inhibitor Y27632 increases branching activity of endothelial cells cultured in a collagen gel (Fischer *et al.*, 2009).

Since the initiation of branching is usually observed in an area with reduced NM2 activity, it is proposed that the inhibition of NM2 activity by inhibition of ROCK promotes the initiation of branching. Here our study shows that tip endothelial cells in wild-type sprouts generate blebbing activities and that these blebs are highly dynamic, but usually do not form stable protrusions. Once protruded, they quickly retract. However when NM2A is ablated or NM2 activity is inhibited, the tip cells show no blebbing dynamics, instead they form excessive cortical protrusions. These results are consistent with the role of NM2 facilitating retraction of cortical protrusions, rather than inhibiting the initiation of cortical protrusions. This is further supported by our findings that the intensity of NM2A increases during retraction of cortical protrusion. The role of NM2 in the retraction of cortical protrusions has been proposed during border cell migration in *Drosophila* showing that loss of NM2 leads to the development of multiple cortical protrusions causing a defect in directional migration of the border cells (Mishra *et al.*, 2019). Similar to NM2’s role in protrusion retraction in migrating cells, NM2 drives membrane integration into the apical plasma membrane of large secretory granules following exocytosis in the salivary gland (Milberg *et al.*, 2017). Alternatively, instead of a role for NM2 in maintaining cortical stability, NM2 may in general regulate cytoskeletal structures. Ablation of NM2 disrupts actomyosin stress-fiber formation and stabilizes microtubules, thereby altering mechanical properties of the cell cortex. Disruption of actomyosin structures could lead to the release of monomeric actin from stress-fibers which then provides an extra pool available for actin nucleators to drive cortical protrusion (Lomakin *et al.*, 2015; Rotty *et al.*, 2015; Suarez *et al.*, 2015; Beach *et al.*, 2017). Delineating this possibility will be very important in the future.

Failure to prevent excessive cortical protrusions not only leads to the increased branching of blood vessels seen in NM2 ablated mice, it also impairs persistence of directed collective sprouting as

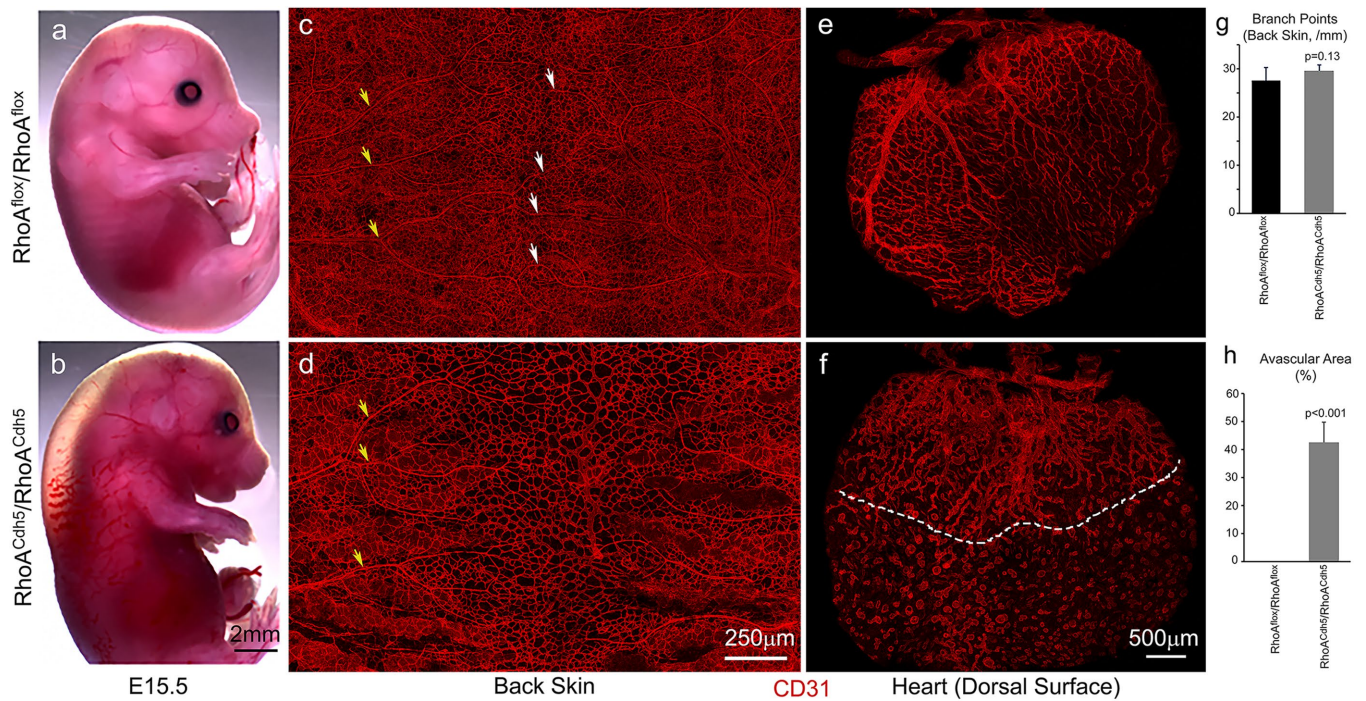


FIGURE 9: Abnormal blood vessel formation in tamoxifen-induced (E10.5) endothelial RhoA-ablated mouse embryos at E15.5. (a, b) Images of control, a (RhoA^{fllox}/RhoA^{fllox}) and endothelial RhoA-ablated, b (RhoA^{Cdh5}/RhoA^{Cdh5}) mouse embryos at E15.5 show that endothelial specific ablation of RhoA in mice results in edema and hemorrhages, b, which are not seen in control littermates, a. (c, d) Wholemount confocal images of E15.5 mouse back skin stained with CD31 antibodies show that blood vessels cover the entire back skin in RhoA^{fllox}/RhoA^{fllox}, c, and RhoA^{Cdh5}/RhoA^{Cdh5} mice, d. Mature remodeled blood vessels are observed in both lateral and middle regions in RhoA^{fllox}/RhoA^{fllox} mice—c, yellow and white arrows, respectively. Mature remodeled vessels are observed in the lateral region (yellow arrows), but are not found at the middle region in the RhoA ablated RhoA^{Cdh5}/RhoA^{Cdh5} mice, d. (e, f) Wholemount confocal images of coronary vessels at the dorsal surface of E15.5 mouse hearts stained with CD31 antibodies show that the coronary vessels cover the entire dorsal surface in RhoA^{fllox}/RhoA^{fllox} hearts, e. The coronary vessels are only seen at the basal area, but fail to grow through the middle of the dorsal surface in RhoA^{Cdh5}/RhoA^{Cdh5} hearts, f. Panel g quantified the average branch points of RhoA^{fllox}/RhoA^{fllox} and RhoA^{Cdh5}/RhoA^{Cdh5} back skin vasculatures. $n = 4$ each, $p = 0.13$ (not statistically significantly different). Panel h quantifies the avascular areas of RhoA^{fllox}/RhoA^{fllox} and RhoA^{Cdh5}/RhoA^{Cdh5} hearts. $n = 3$ each, $p < 0.0001$.

manifested by frequent changes of migration directions. The impaired directional migration could contribute to the delayed vascular coverage seen in NM2 ablated mice. NM2 regulation of the direction of cell migration has been demonstrated both in vivo, such as in germ cell migration in zebrafish (Blaser *et al.*, 2006) and in cultured MEF cells (Conti *et al.*, 2004; Lo *et al.*, 2004). Ablation of NM2 or inhibition of NM2 activity impairs the persistence of migration, but does not affect (often even increases) the speed of cell movement. During collective cell migration, the leader cells positioned at the front generate lamellipodial and filopodial protrusions, which sense, lead and power the migration (Reffay *et al.*, 2014; Mayor and Etienne-Manneville, 2016). NM2 contributes to the traction forces at the front of migration, as well as to stabilization of the cortical surface to steer the direction of migration. Our results from EB angiogenic sprouting show that ablation of NM2 affects the directionality, but not the speed of sprouting migration. Thus NM2 plays a major role in maintaining the persistence of migration in vascular sprouting. In a 3D biomimetic model of angiogenesis using HUVECs, Yoon *et al.* (2019) reported that deletion of NM2A expression or inhibition of NM2 by blebbistatin led to scattering of HUVECs from sprouts, but does not affect cell invasion (Yoon *et al.*, 2019). In our study of mice in vivo and in EB sprouting in culture, we do not see remarkable scattering of endothelial cells in NM2 ablated or blebbistatin

treated sprouts. This may partially be due to the difference of our experimental models. Using 3D sprouting of HUVEC aggregates in collagen gels, we also find that inhibition of NM2 by blebbistatin or Y27632 results in cell scattering from sprouts and disruption of VE-cadherin junctions in sprouts (our unpublished data).

NM2 ablation in endothelial cells affects directional migration and sprouting activity during vascular development, however, the general pattern of the developing vasculature is not affected either in the back skin or the heart. Therefore NM2 is not required for sensing during vascular sprouting. It is believed that lamellipodial and filopodial structures function to sense the angiogenic stimulus thereby guiding vascular sprouts (Gerhardt *et al.*, 2003; Lamalice *et al.*, 2007; De Smet *et al.*, 2009). NM2 is one of the major cytoplasmic motors regulating lamellipodial and filopodial structures (Burnette *et al.*, 2011; Alieva *et al.*, 2019). Ablation of NM2 or inhibition of NM2 activity greatly disrupts filopodium formation and lamellipodium dynamics in vascular sprouts, but does not affect vascular sprouting toward its destination. Therefore, NM2 regulation of endothelial filopodial and lamellipodial structures is not important for sensing the angiogenic stimulus during angiogenesis. Whether filopodia and lamellipodia are important or other regulators are required for sensing remains to be determined.

Our results also reveal that the relative contribution of NM2 paralogs to the development of the skin vasculature and cardiac coronary vasculature is not the same. Although NM2A in general plays the major role, the contribution of NM2B is more significant in coronary vascular development compared with skin vascular development. In addition, RhoA activated Rho kinase is important for coronary vascular development, but is not as important for the skin vasculature. Different contribution of NM2B in the regulation of the skin and coronary vasculatures may partially be related to the different mechanical environments of the developing vasculatures between the skin and heart. The cardiac coronary vasculature encounters a relative stiff environment compared with the skin vasculature. On the other hand, NM2B is more suitable to generate sustained tension and shows an increased mechanoresponsiveness due to its prolonged duty-ratio and increased load-dependent force generation, when compared with NM2A (Kovacs *et al.*, 2007; Billington *et al.*, 2013; Schifffhauer *et al.*, 2019). This is consistent with the idea that vascular development in different organs is regulated by different signaling pathways and molecular motors.

MATERIALS AND METHODS

Animals

A^{flox}/A^{flox}, B^{flox}/B^{flox}, B⁻/B⁻, A^{GFP}/A^{GFP}, and B^{GFP}/B^{GFP} mice were generated as previously described (Tullio *et al.*, 1997; Bao *et al.*, 2007; Ma *et al.*, 2009; Jacobelli *et al.*, 2010; Zhang *et al.*, 2012) and are available through the Mutant Mouse Regional Resource Centers (MMRRC: #032096, #016981, #16991, #037506, and #037053). RhoA^{flox}/RhoA^{flox} mice were generated as previously reported (Melendez *et al.*, 2011). Tie2-cre mice were obtained from Jackson Laboratory (stock #004128). Cdk5-CreER mice were generated as described (Okabe *et al.*, 2014). To obtain homozygous ablated mice (flox/flox;Cre+), a heterozygous male containing one allele of Cre (+/flox;Cre+/-) was crossed with a double-floxed female (flox/flox). Therefore the homozygous ablated mouse only expressed one Cre allele. All procedures were conducted using an approved animal protocol (H0053R3) in accordance with National Heart, Lung, and Blood Institute Animal Care and Use Committee guidelines.

Wholemout immunofluorescence staining of vasculature

Mouse embryos were collected in phosphate-buffered saline (PBS) and directly immersed in 4% paraformaldehyde (PFA) in PBS (pH 7.4) at 4°C overnight. Following fixation, the samples were washed with PBS and stored in PBS at 4°C for further analyses. Back skins and hearts were dissected from fixed embryos and then stained by wholemount immunofluorescence staining as previously described (Yamazaki *et al.*, 2017). The following primary antibodies were used in this study: polyclonal antibodies against NMHC 2A (1:1,000, Biologend), NMHC2B (1:3,000, Biologend), p-paxillin (1:1,000; BD Transduction Laboratories); monoclonal antibodies against PECAM1 (CD31, 1:200, BD Pharmingen), GFP (1:200, ab183734, Abcam). Fluorescence secondary antibodies used were Alexa 488 goat anti-rabbit IgG or Alexa 594 goat anti-mouse IgG (1:250, Invitrogen, Carlsbad, CA). Confocal microscopy was carried out either on a Leica TCS SP5 or on a Zeiss LSM 880. In all cases, when possible, comparison was made among littermates. For each genotype we analyzed at least three to five mice. We found no abnormalities in NM2A and NM2B single heterozygous mice or NM2A/2B double heterozygous mice compared with the littermates that expressed no Cre. Littermates containing no cre recombinase were used as controls for conditional ablated mice.

In vitro EB angiogenic sprouting

EB angiogenic sprouting was performed as previously described (Jakobsson *et al.*, 2010). Mouse embryonic stem (ES) cells were cultured in gelatin-coated culture dishes containing 100 U/ml leukemia inhibitory factor in ES culture medium. EB were prepared in a low-attachment 96-well plate. 500 ES cells (in 200 µl volume) were added into each well and cultured in differentiating medium (ES medium without LIF) for 4 d. EB were then collected and sandwiched in 1.5% collagen I gel (Purecol, INAMED biomaterials) to induce angiogenic sprouting in differentiation medium containing 30 ng/ml recombinant VEGFA-165 (Preprotech) in a 12-well culture plate. The sprouts were fixed in 4%PFA and analyzed by staining with the various antibodies at 7 d after culture. For live cell imaging, sprouts were analyzed between days 3 and 5 using an Olympus X-70 microscope.

Quantification and statistical analyses

AngioTool (Zudaire *et al.*, 2011) was used to characterize the vasculature in the back skin and in vitro EB angiogenic sprouting following CD31 staining to reveal the vascular network. NIH ImageJ was used to analyze live cell imaging, fluorescence intensity of staining, and avascular areas. Data are expressed as means ± SD. Student's *t* test was performed to compare two means. One-way ANOVA (post-Tukey) was used when comparing more than two means.

ACKNOWLEDGMENTS

We thank Mary Anne Conti and Sachiyo Kawamoto and members of the Laboratory of Molecular Cardiology for their critical comments on the manuscript. We also thank Fang Zhang and Yubin Du (National Heart, Lung, and Blood Institute [NHLBI] Transgenic Core) and Christian A. Combs and Daniela Malide (NHLBI Light Microscopy Core). Dalton Saunders provided technical assistance.

REFERENCES

- Abraham S, Yeo M, Montero-Balaguer M, Paterson H, Dejana E, Marshall CJ, Mavria G (2009). VE-cadherin-mediated cell-cell interaction suppresses sprouting via signaling to MLC2 phosphorylation. *Curr Biol* 19, 668–674.
- Alieva NO, Efremov AK, Hu S, Oh D, Chen Z, Natarajan M, Ong HT, Jegou A, Romet-Lemonne G, Groves JT, *et al.* (2019). Myosin IIA and formin dependent mechanosensitivity of filopodia adhesion. *Nat Commun* 10, 3593.
- Angulo-Urarte A, Casado P, Castillo SD, Kobiak P, Kotini MP, Figueiredo AM, Castel P, Rajeev V, Mila-Guasch M, Millan J, *et al.* (2018). Endothelial cell rearrangements during vascular patterning require PI3-kinase-mediated inhibition of actomyosin contractility. *Nat Commun* 9, 4826.
- Bao J, Ma X, Liu C, Adelstein RS (2007). Replacement of nonmuscle myosin II-B with II-A rescues brain but not cardiac defects in mice. *J Biol Chem* 282, 22102–22111.
- Beach JR, Bruun KS, Shao L, Li D, Swider Z, Remmert K, Zhang Y, Conti MA, Adelstein RS, Rusan NM, *et al.* (2017). Actin dynamics and competition for myosin monomer govern the sequential amplification of myosin filaments. *Nat Cell Biol* 19, 85–93.
- Beach JR, Shao L, Remmert K, Li D, Betzig E, Hammer JA 3rd (2014). Nonmuscle myosin II isoforms coassemble in living cells. *Curr Biol* 24, 1160–1166.
- Berg JS, Powell BC, Cheney RE (2001). A millennial myosin census. *Mol Biol Cell* 12, 780–794.
- Billington N, Wang A, Mao J, Adelstein RS, Sellers JR (2013). Characterization of three full-length human nonmuscle myosin II paralogs. *J Biol Chem* 288, 33398–33410.
- Blaser H, Reichman-Fried M, Castanon I, Dumstrei K, Marlow FL, Kawakami K, Solnica-Krezel L, Heisenberg CP, Raz E (2006). Migration of zebrafish primordial germ cells: a role for myosin contraction and cytoplasmic flow. *Dev Cell* 11, 613–627.
- Bryan BA, Dennstedt E, Mitchell DC, Walshe TE, Noma K, Loureiro R, Saint-Geniez M, Campaigniac JP, Liao JK, D'Amore PA (2010). RhoA/ROCK signaling is essential for multiple aspects of VEGF-mediated angiogenesis. *FASEB J* 24, 3186–3195.

- Burnette DT, Manley S, Sengupta P, Sougrat R, Davidson MW, Kachar B, Lippincott-Schwartz J (2011). A role for actin arcs in the leading-edge advance of migrating cells. *Nat Cell Biol* 13, 371–381.
- Cao J, Ehling M, Marz S, Seebach J, Tarbashevich K, Sixta T, Pitulescu ME, Werner AC, Flach B, Montanez E, et al. (2017). Polarized actin and VE-cadherin dynamics regulate junctional remodelling and cell migration during sprouting angiogenesis. *Nat Commun* 8, 2210.
- Carmeliet P, Jain RK (2011). Molecular mechanisms and clinical applications of angiogenesis. *Nature* 473, 298–307.
- Conti MA, Even-Ram S, Liu C, Yamada KM, Adelstein RS (2004). Defects in cell adhesion and the visceral endoderm following ablation of non-muscle myosin heavy chain II-A in mice. *J Biol Chem* 279, 41263–41266.
- Cukierman E, Pankov R, Stevens DR, Yamada KM (2001). Taking cell–matrix adhesions to the third dimension. *Science* 294, 1708–1712.
- De Smet F, Segura I, De Bock K, Hohensinner PJ, Carmeliet P (2009). Mechanisms of vessel branching: filopodia on endothelial tip cells lead the way. *Arterioscler Thromb Vasc Biol* 29, 639–649.
- Eilken HM, Adams RH (2010). Dynamics of endothelial cell behavior in sprouting angiogenesis. *Curr Opin Cell Biol* 22, 617–625.
- Even-Ram S, Doyle AD, Conti MA, Matsumoto K, Adelstein RS, Yamada KM (2007). Myosin IIA regulates cell motility and actomyosin–microtubule crosstalk. *Nat Cell Biol* 9, 299–309.
- Fischer RS, Gardel M, Ma X, Adelstein RS, Waterman CM (2009). Local cortical tension by myosin II guides 3D endothelial cell branching. *Curr Biol* 19, 260–265.
- Gaengel K, Niaudet C, Hagikura K, Lavina B, Muhl L, Hofmann JJ, Ebarasi L, Nyström S, Rymo S, Chen LL, et al. (2012). The sphingosine-1-phosphate receptor S1PR1 restricts sprouting angiogenesis by regulating the interplay between VE-cadherin and VEGFR2. *Dev Cell* 23, 587–599.
- Gerhardt H, Golding M, Fruttiger M, Ruhrberg C, Lundkvist A, Abramsson A, Jeltsch M, Mitchell C, Alitalo K, Shima D, Betsholtz C (2003). VEGF guides angiogenic sprouting utilizing endothelial tip cell filopodia. *J Cell Biol* 161, 1163–1177.
- Golomb E, Ma X, Jana SS, Preston YA, Kawamoto S, Shoham NG, Goldin E, Conti MA, Sellers JR, Adelstein RS (2004). Identification and characterization of nonmuscle myosin II-C, a new member of the myosin II family. *J Biol Chem* 279, 2800–2808.
- Heissler SM, Manstein DJ (2013). Nonmuscle myosin-2: mix and match. *Cell Mol Life Sci* 70, 1–21.
- Heuze ML, Sankara Narayana GHN, D’Alessandro J, Cellerin V, Dang T, Williams DS, Van Hest JC, Marq P, Mege RM, Ladoux B (2019). Myosin II isoforms play distinct roles in adherens junction biogenesis. *Elife* 8.
- Hoelzle MK, Svitkina T (2012). The cytoskeletal mechanisms of cell–cell junction formation in endothelial cells. *Mol Biol Cell* 23, 310–323.
- Jacobelli J, Friedman RS, Conti MA, Lennon-Dumenil AM, Piel M, Sorensen CM, Adelstein RS, Krummel MF (2010). Confinement-optimized three-dimensional T cell amoeboid motility is modulated via myosin IIA-regulated adhesions. *Nat Immunol* 11, 953–961.
- Jakobsson L, Franco CA, Bentley K, Collins RT, Ponsioen B, Aspalter IM, Rosewell I, Busse M, Thurston G, Medvinsky A, et al. (2010). Endothelial cells dynamically compete for the tip cell position during angiogenic sprouting. *Nat Cell Biol* 12, 943–953.
- Kamijo H, Matsumura Y, Thumkeo D, Koike S, Masu M, Shimizu Y, Ishizaki T, Narumiya S (2011). Impaired vascular remodeling in the yolk sac of embryos deficient in ROCK-I and ROCK-II. *Genes Cells* 16, 1012–1021.
- Kovacs M, Thirumurugan K, Knight PJ, Sellers JR (2007). Load-dependent mechanism of nonmuscle myosin 2. *Proc Natl Acad Sci USA* 104, 9994–9999.
- Kroll J, Epting D, Kern K, Dietz CT, Feng Y, Hammes HP, Wieland T, Augustin HG (2009). Inhibition of Rho-dependent kinases ROCK I/II activates VEGF-driven retinal neovascularization and sprouting angiogenesis. *Am J Physiol Heart Circ Physiol* 296, H893–H899.
- Lamallice L, Le Boeuf F, Huot J (2007). Endothelial cell migration during angiogenesis. *Circ Res* 100, 782–794.
- Liu J, Wada Y, Katsura M, Tozawa H, Erwin N, Kapron CM, Bao G, Liu J (2018). Rho-associated coiled-coil kinase (ROCK) in molecular regulation of angiogenesis. *Theranostics* 8, 6053–6069.
- Liu Z, Tan JL, Cohen DM, Yang MT, Sniadecki NJ, Ruiz SA, Nelson CM, Chen CS (2010). Mechanical tugging force regulates the size of cell–cell junctions. *Proc Natl Acad Sci USA* 107, 9944–9949.
- Lo CM, Buxton DB, Chua GC, Dembo M, Adelstein RS, Wang YL (2004). Nonmuscle myosin IIb is involved in the guidance of fibroblast migration. *Mol Biol Cell* 15, 982–989.
- Lomakin AJ, Lee KC, Han SJ, Bui DA, Davidson M, Mogilner A, Danuser G (2015). Competition for actin between two distinct F-actin networks defines a bistable switch for cell polarization. *Nat Cell Biol* 17, 1435–1445.
- Ma X, Adelstein RS (2014). The role of vertebrate nonmuscle Myosin II in development and human disease. *Bioarchitecture* 4, 88–102.
- Ma X, Jana SS, Conti MA, Kawamoto S, Claycomb WC, Adelstein RS (2010). Ablation of nonmuscle myosin II-B and II-C reveals a role for nonmuscle myosin II in cardiac myocyte karyokinesis. *Mol Biol Cell* 21, 3952–3962.
- Ma X, Sung DC, Yang Y, Wakabayashi Y, Adelstein RS (2017). Nonmuscle myosin IIB regulates epicardial integrity and epicardium-derived mesenchymal cell maturation. *J Cell Sci* 130, 2696–2706.
- Ma X, Takeda K, Singh A, Yu ZX, Zervas P, Blount A, Liu C, Towbin JA, Schneider MD, Adelstein RS, Wei Q (2009). Conditional ablation of nonmuscle myosin II-B delineates heart defects in adult mice. *Circ Res* 105, 1102–1109.
- Mayor R, Etienne-Manneville S (2016). The front and rear of collective cell migration. *Nat Rev Mol Cell Biol* 17, 97–109.
- Melendez J, Stengel K, Zhou X, Chauhan BK, Debidda M, Andreassen P, Lang RA, Zheng Y (2011). RhoA GTPase is dispensable for actomyosin regulation but is essential for mitosis in primary mouse embryonic fibroblasts. *J Biol Chem* 286, 15132–15137.
- Milberg O, Shitara A, Ebrahim S, Masedunskas A, Tora M, Tran DT, Chen Y, Conti MA, Adelstein RS, Ten Hagen KG, Weigert R (2017). Concerted actions of distinct nonmuscle myosin II isoforms drive intracellular membrane remodeling in live animals. *J Cell Biol* 216, 1925–1936.
- Mishra AK, Mondo JA, Campanale JP, Montell DJ (2019). Coordination of protrusion dynamics within and between collectively migrating border cells by myosin II. *Mol Biol Cell* 30, 2490–2502.
- Okabe K, Kobayashi S, Yamada T, Kurihara T, Tai-Nagara I, Miyamoto T, Mukoyama YS, Sato TN, Suda T, Ema M, Kubota Y (2014). Neurons limit angiogenesis by titrating VEGF in retina. *Cell* 159, 584–596.
- Park JA, Atia L, Mitchel JA, Fredberg JJ, Butler JP (2016). Collective migration and cell jamming in asthma, cancer and development. *J Cell Sci* 129, 3375–3383.
- Phng LK, Gerhardt H (2009). Angiogenesis: a team effort coordinated by notch. *Dev Cell* 16, 196–208.
- Reffay M, Parrini MC, Cochet-Escartin O, Ladoux B, Buguin A, Coscoy S, Amblard F, Camonis J, Silberzan P (2014). Interplay of RhoA and mechanical forces in collective cell migration driven by leader cells. *Nat Cell Biol* 16, 217–223.
- Rotty JD, Wu C, Haynes EM, Suarez C, Winkelmann JD, Johnson HE, Haugh JM, Kovar DR, Bear JE (2015). Profilin-1 serves as a gatekeeper for actin assembly by Arp2/3-dependent and -independent pathways. *Dev Cell* 32, 54–67.
- Sauteur L, Krudewig A, Herwig L, Ehrenfeuchter N, Lenard A, Affolter M, Belting HG (2014). Cdh5/VE-cadherin promotes endothelial cell interface elongation via cortical actin polymerization during angiogenic sprouting. *Cell Rep* 9, 504–513.
- Schiffhauer ES, Ren Y, Iglesias VA, Kothari P, Iglesias PA, Robinson DN (2019). Myosin IIB assembly state determines its mechanosensitive dynamics. *J Cell Biol* 218, 895–908.
- Shutova MS, Spessott WA, Giraudo CG, Svitkina T (2014). Endogenous species of mammalian nonmuscle myosin IIA and IIB include activated monomers and heteropolymers. *Curr Biol* 24, 1958–1968.
- Smutny M, Cox HL, Leerberg JM, Kovacs EM, Conti MA, Ferguson C, Hamilton NA, Parton RG, Adelstein RS, Yap AS (2010). Myosin II isoforms identify distinct functional modules that support integrity of the epithelial zonula adherens. *Nat Cell Biol* 12, 696–702.
- Suarez C, Carroll RT, Burke TA, Christensen JR, Bestul AJ, Sees JA, James ML, Sirotkin V, Kovar DR (2015). Profilin regulates F-actin network homeostasis by favoring formin over Arp2/3 complex. *Dev Cell* 32, 43–53.
- Szymborska A, Gerhardt H (2018). Hold me, but not too tight—endothelial cell–cell junctions in angiogenesis. *Cold Spring Harb Perspect Biol* 10.
- Takeda K, Kishi H, Ma X, Yu ZX, Adelstein RS (2003). Ablation and mutation of nonmuscle myosin heavy chain II-B results in a defect in cardiac myocyte cytokinesis. *Circ Res* 93, 330–337.
- Tullio AN, Accili D, Ferrans VJ, Yu ZX, Takeda K, Grinberg A, Westphal H, Preston YA, Adelstein RS (1997). Nonmuscle myosin II-B is required for normal development of the mouse heart. *Proc Natl Acad Sci USA* 94, 12407–12412.
- Tullio AN, Bridgman PC, Tresser NJ, Chan CC, Conti MA, Adelstein RS, Hara Y (2001). Structural abnormalities develop in the brain after ablation of the gene encoding nonmuscle myosin II-B heavy chain. *J Comp Neurol* 433, 62–74.

- Wang A, Ma X, Conti MA, Liu C, Kawamoto S, Adelstein RS (2010). Nonmuscle myosin II isoform and domain specificity during early mouse development. *Proc Natl Acad Sci USA* 107, 14645–14650.
- Wimmer R, Cseh B, Maier B, Scherrer K, Baccharini M (2012). Angiogenic sprouting requires the fine tuning of endothelial cell cohesion by the Raf-1/Rok-alpha complex. *Dev Cell* 22, 158–171.
- Yamazaki T, Nalbandian A, Uchida Y, Li W, Arnold TD, Kubota Y, Yamamoto S, Ema M, Mukoyama YS (2017). Tissue myeloid progenitors differentiate into pericytes through TGF-beta signaling in developing skin vasculature. *Cell Rep* 18, 2991–3004.
- Yoon C, Choi C, Stapleton S, Mirabella T, Howes C, Dong L, King J, Yang J, Oberai A, Eyckmans J, Chen CS (2019). Myosin IIA-mediated forces regulate multicellular integrity during vascular sprouting. *Mol Biol Cell* 30, 1974–1984.
- Zhang Y, Conti MA, Malide D, Dong F, Wang A, Shmist YA, Liu C, Zerfas P, Daniels MP, Chan CC, et al. (2012). Mouse models of MYH9-related disease: mutations in nonmuscle myosin II-A. *Blood* 119, 238–250.
- Zhang Y, Liu C, Adelstein RS, Ma X (2018). Replacing nonmuscle myosin 2A with myosin 2C1 permits gastrulation but not placenta vascular development in mice. *Mol Biol Cell* 29, 2326–2335.
- Zudaire E, Gambardella L, Kurcz C, Vermeren S (2011). A computational tool for quantitative analysis of vascular networks. *PLoS One* 6, e27385.